Comparative Experimental and Theoretical Study on the Structure of Potassium 2,4-Hexadienoate: Structure-Activity Relationship

Manel Taferguennit
University of Sciences and Technology Houari Boumediene

Noura Kichou
University of Mouloud Mammeri of Tizi-Ouzou

Zakia Hank
University of Sciences and Technology Houari Boumediene

Abstract: For the first time, a density functional theory (DFT) study was conducted on the structure of a well-known antibacterial agent namely potassium 2,4-Hexadienoate, in order to elucidate its vibrational, electronic and reactivity proprieties. Structure optimization was performed using three common hybrid functionals (DFT/B3LYP-D3; DFT/ M05-2X and DFT/M06-2X) to identify the suitable functional. Geometric parameters, IR and UV-vis spectra were well reproduced when using DFT/M06-2X with 6-311(d)G+ basis set ($R2 = 0.99913$). The assimilation of IR frequencies has been achieved using potential energy distribution (PED)analysis at M06-2X/6-311(d) G + level. Time-dependent density functional theory (TD-DFT) and natural bond orbital (NBO) analysis were realized to identify the excited states of 2,4-Hexadienoate anion in the liquid phase, using the solute electron density solvation model (SMD). Moreover, reactive sites in the molecule were localized by molecular electrostatic potential (MEP) analysis. Highest Occupied Molecular Orbitals (HOMO), lowest Unoccupied Molecular Orbitals (LUMO) and energy gap (HOMO-LUMO gap), were used to calculate global reactivity descriptors (GRDs), according to the frontier molecular orbitals (FMO) theory, the resulting values were analyzed to explore the chemical reactivity of the molecule and elucidate the structure-activity relationship.

Keywords: Sorbate, DFT, HOMO-LUMO gap, NBO, Antimicrobial activity.

Introduction

Organic molecules are becoming widespread for practical applications in pharmaceutical fields (Salami & Shokri, 2021). Those molecules exist in the environment in the form of low molecular weight, small chain molecules, containing both carbon and hydrogen, and often other elements like oxygen, such as in organic acids (Strathmann & Myneni, 2004), (Reichle, 2020). Initially, organic acids are compounds that occur naturally from animal and plants sources. They are classified according to four characteristics: (1) carbon chain nature (cyclic, acyclic, alicyclic, and heterocyclic); (2) saturated or unsaturated chain; (3) the existence or inexistence of substituents ; and (4) the number of carboxyl moiety (mono, di- or tri-carboxylic) (Chahardoli et al., 2020).

Previous research revealed the impressive effectiveness of organic acids such as benzoic acids, parabens, sorbic acid and their salts (i.e., sorbates, benzoates, propionates) against many microbial species including bacterial strains, yeast and molds (Baldevraj & Jagadish, 2011). Nowadays, sorbates are the 3rd most important group of antimicrobial food and pharmaceutical preservatives, after parabens and benzoates, whose safety has been discussed by recent publications (Mackowiak-Dryka et al., 2015; Piper, 2018). Although the antibacterial mechanism of sorbate is fully defined, its biological activity is often associated with its chemical structure

(Davidson, 2005). The carboxyl group and the conjugated double bonds in this molecule are highly reactive (Davidson, 2005) . In *Escherichia coli,* the mechanism of action of potassium sorbate consists of binding to enzymes related to the glycolysis metabolism, the Krebs cycle, and electron active transport (Santiesteban-López et al., 2009) such as Enolase, Aspartase, Catalase, and Malate Dehydrogenase., by blocking their active sites, the assimilation of important substrates is thus decreased, causing the inhibition of *Escherichia coli* growth and its death (Santiesteban-López et al., 2009). Computational approaches have received great attention in understanding the relationship between chemical structure and biological activity of studied compounds, commonly called Structure-Activity Relationship (SAR) (Guerrero-Perilla et al., 2015), (Kalhotra et al., 2018).

SAR analysis can be employed to develop more effective and targeted bioactive molecules by improving them and analyzing the various ways in which they binds to a receptor(James, 2022).There are numerous computational techniques that can identify the SAR,including physicochemical properties determination and drug-receptor interaction analysis using molecular docking.The physicochemical properties are computed to investigate one of the most common biological property i.e., "the bioavailability"in order to understand the Structure-Activity Relationship (SAR)(James, 2022), (D'Souza et al., 2009). In another hand, molecular docking predicts the position of a ligand, as an inhibitor of the target protein in its binding site, as well as the accurate estimation of the binding strength and the number and the nature of the involved interactions. It worth mentioning docking results accuracy is highly dependent to preparation conditions such as optimization of the structure of both of the ligand and the protein (Zaater et al., 2016). Based on the literature survey, no study was carried out applying computational methods to explain the antibacterial activity of sorbates.

Therefore, the current study is focused on the use of computational calculations to elucidate the structure-activity relationship in the case of potassium sorbate. Theoretical calculations, by means of DFT/B3LYP approach, were initially carried out in order to prepare the structure to molecular docking. Three common density theory functionals i.e., *B3LYP-D3*, *M05-2X*and *M06-2X* were tested, the calculated data were compared to the experimental data, the optimized structure with the appropriate functional was chosen to provide further structural characteristics such as molecular descriptors, highest occupied molecular orbital, molecular electrostatic potential mapping and chemical reactivity. The optimized structure of potassium sorbate was docked in the binding site of glycolytic metalloenzyme "Enolase" from E. coli (PDB: 6BFZ (Bank, 1971.)), all the involved interactions with the target protein residues were visualized.Furthermore, In here, physicochemical properties are predicted in silico using SwissADME server (Daina et al., 2017).

Method

For the purpose of the analysis, a Jasco FTIR 6000 Series Spectrometer recorded FT-IR spectra (4000-400 cm^{-1}) using potassium bromide pallet. A Jasco V-700 Series UV-VIS/NIR Spectrophotometer measured the electronic spectra from 200 to 800nm. Theoretical calculations of the structure of the sorbate molecule were realized using *Gaussian 09* program package (Liang et al, 2009), by the employment of three common density theory functionals: *B3LYP-D3*(Grimme et al., 2011), *M05-2X* (Dimić et al., 2018) and *M06-2X*(Zhao & Truhlar, 2008). The GaussView program v5.0.8 was employed to display the input files. After the verification of the absence of imaginary frequencies, the optimized structure of sorbate with the appropriate functional is ready to be docked into the target protein. Enolase metalloenzyme was chosen as a target protein. Its crystal structure of into the active site of glycolytic metalloenzyme "Enolase" from E. coli (PDB: 6BFZ (Bank, 1971)) was retrieved from protein data bank (PDB) (Kleeb, 2015).

Molecular docking was done using Molecular Operating Environment (MOE) 2015.10 software (Chemical Computing Group, Montreal, Canada, 2015). The structure of the Enolase was prepared with MOE QuikPrep tool at default parameters, where the co-crystalized ligand and all water molecules that are farther than 4.5 Å from the enzyme were removed, except the co-factor Mg(II), all necessary hydrogen atoms were added to the structure, followed by its energy optimization. The prepared Enolase enzyme structure and the optimized sorbate were subject to a number of docking runs. The best binding conformation was selected based by following to "standard" docking solutions considered as typical in docking analysis i.e., (1) the minimal binding energy, that reflects the best docking pose, (2) the lowest with lowest root mean square deviation (RMSD) value that validate the docking process (Angelova et al., 2017), (Alomari, 2018).

A protein-ligand interactions diagram was constructed based on the best binding pose, using Ligand interactions entry in MOE software. The interactions were detected in the maximum distance of 4.5 Å; between heavy atoms of the ligand and the receptor residues (Angelova et al., 2017), and their nature was identified according to the diagram legend given in Ligand interactions entry.The ability of molecules to produce biological effect is

dependent on the impact of various physicochemicalproperties of the bioactive molecule on the protein with which it interacts(ALGHAMDI et al., 2020). In here, physicochemical properties are predicted in silico using SwissADME server (Daina et al., 2017).

Results and Discussion

Optimization of the Molecular Structure

In order to define the most appropriate functional for the optimization, different density functional theory hybrids were used, including *DFT/B3LYP-D3*(Grimme et al., 2011), *DFT/M05-2X*(Dimić et al., 2018) and *DFT/M06-2X*(Zhao & Truhlar, 2008) with *6-311+G(d)* basis set (Grimme et al., 2011). Analogous association has been used to provide a good description of similar molecular systems and to reproduce their spectra (Mehandzhiyski et al., 2015),(Sert et al., 2015). Before optimization, the BSEE counterpoise correction method was used to adjust the interaction energies between the potassium cation and the sorbate anion (Mehta & Goerigk, 2021). The structure of the compound was optimized without any structural constraints and the inexistence of negative frequencies values proved that the obtained structure was in the minima energy state.

Optimized structure parameters (bond lengths, bond and dihedrals angles) were compared with the experimental corresponding values and illustrated in Table 1. Due to unavailability of experimental data, the main structural parameters of the present compound have been compared to similar systems with solved crystal structures. (Schlitter & Beck, 1996). The structure and the atom numbering of potassium sorbate is reported in Figure 1.
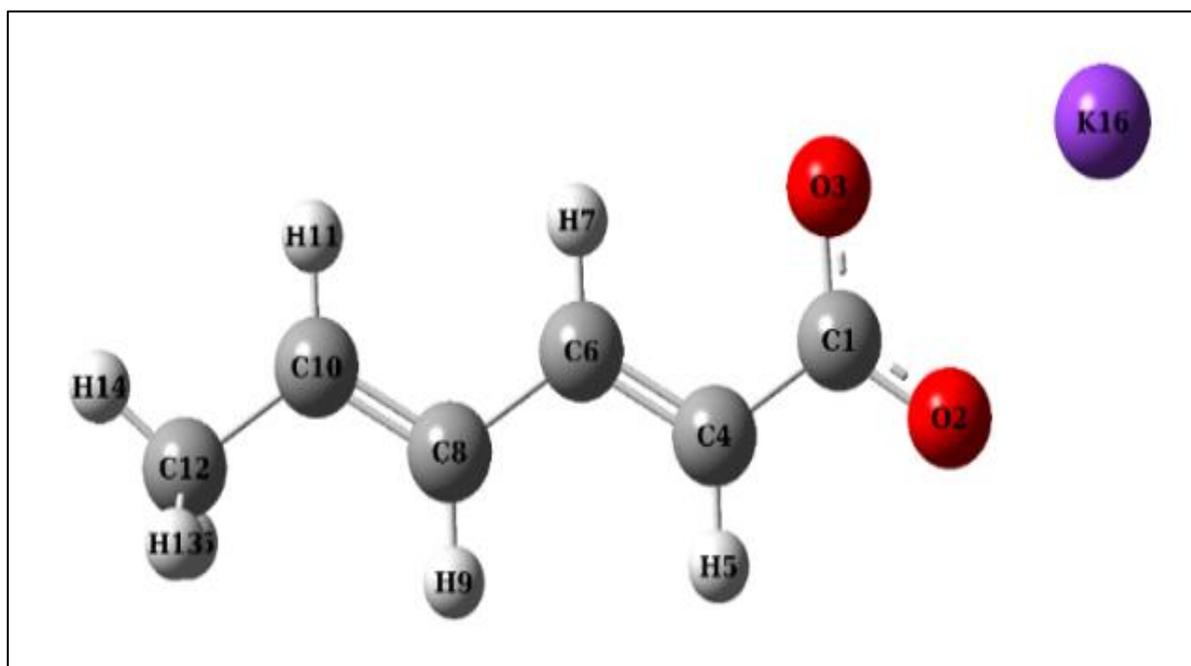

Figure 1. Molecular structure of potassium sorbate.

As the optimization was done in the gas phase, the optimized structure parameters calculated by the three functionals are shown to be either slightly longer or shorter than the experimental values obtained in solid phase (Sert, Singer, et al., 2014). From Table 1, it can be seen that the C-C bond lengths of C4-C6 and C8-C10 calculated with *B3LYP-D3*, *M05-2X* and *M06-2X* levels, were restricted in the range 1.335-1.342 Å, characterizing the C-C double bond lengths, which was found around 1.318 Å experimentally. In the carboxylate group of the title molecule, the calculated C1-O3 and C1-O2 bond lengths were found at 1.270 Å (*B3LYP-D3*), 1.263 Å (*M05-2X*) and 1.262 Å (*M06-2X*), these bond lengths were experimentally found to be 1.261 Å as to O2-C1-O3 bond angle was computed at 124.01° (*B3LYP-D3*), 124.22° (*M05-2X*) and 124.35 ° (*M06-2X*). These bond angles were experimentally found to be 123.3°. Although, the calculated C-H bond lengths of CH_3 group, ranging from 1.088 to 1.097 Å, are slightly far from the experimental values, H-C-H bond angle computed values are quietly close to experimental values.

Table1. Computed structural parameters for potassium sorbate

	B3LYP-D3/ 6-311(d) G+	M05-2X/ 6-311(d) G+	M06-2X/ 6-311(d) G+	*Experimental
Bond lengths (Å)				
C1-O2	1.270	1.263	1.262	1 .261
C1-O3	1.271	1.263	1.262	1.267
C1-C4	1.494	1.493	1.498	1.480
C4-C6	1.342	1.335	1.336	1.318
C4-H5	1.087	1.083	1.086	0.96
C6-H7	1.088	1.084	1.088	1.00
C6-C8	1.449	1.454	1.455	1.436
C8-H9	1.090	1.086	1.089	0.93
C8-C10	1.342	1.335	1.336	1.302
C10-H11	1.090	1.086	1.089	0.90
C10-C12	1.498	1.495	1.496	1 .486
C12-H13	1.094	1.088	1.094	0.90
C12-H14	1.097	1.091	1.094	1.01
C12-H15	1.097	1.091	1.091	1.00
Bond angles (°)				
O2-C1-O3	124.01	124.22	124.35	123.3
C1 -C4-C6	123.19	122.24	122.33	124.3
C4-C6-C8	124.36	124.02	124.24	126.2
C6-C8-C10	124.04	123.47	123.72	126.7
C8-C10-C12	124.90	124.75	124.95	127.7
C1-C4-H5	115.84	115.98	115.99	110.3
C4-C6-H7	117.75	117.87	117.77	117.3
C6-C8-H9	116.95	117.05	123.72	114
C8-C10-H11	118.38	118.41	118.34	118
H11-C10-C12	116.71	116.83	116.69	114
C10-C12-H14	111.27	111.00	111.09	110
H14-C12-H13	108.12	108.27	106.73	108
H14-C12-H15	106.46	106.86	108.18	113
H15-C12-H13	108.12	108.28	108.18	108
Dihedral angle (°)				
O3-C1-C4-C6	179.99	179.99	179.99	168.6
O3-C1-C4-H5	0	0	0	10.9
O2-C1-C4-H5	179.99	179.99	180.00	169.1
O2-C1-C4-C6	0	0	0	11.4
C1-C4-C6-H7	0	0	0	2
H5-C4-C6-H7	179.99	179.99	179.99	178
H5-C4-C6-C8	0	0	0	0
C1-C4-C6-C8	179.99	179.99	179.99	179.0
C4-C6-C8-H9	0	0	0	3
C4-C6-C8-C10	179.99	179.99	179.99	175.8
C6-C8-C10-H11	0	0	0	4
H7-C6-C8-H9	180.0	179.99	180.00	179
H7-C6-C8-C10	0	0	0	2
C6-C8-C10-C12	179.99	179.99	179.99	179.6

*Lithium sorbate data given in ref (Schlitter & Beck, 1996)

Vibrational Spectral Analysis

The IR data of fundamentals modes in the potassium sorbate molecule were computed at *B3LYP-D3*, *M05-2X* and *M06-2X* levels and listed in Table 2. All the vibrational assignments have been made using the *VEDA* software package,which uses potential energy distribution (PED) analysis for the estimation of normal modes percentage in each frequency (Dimić et al., 2018). The calculated vibrational frequencies have been scaled and all the calculations (vibrational wavenumbers, optimized geometric) were compared with the experimental corresponding results, in order to identify the most suitable functional has been identified.

Table 2. Experimental and computed IR frequencies of potassium sorbate.

Vib. no	Assignement (PED[*]%)	Calc.freq			Exp.freq
		B3LYP-D3 6-311(d)G+ 0.966 (*CCCBDB Listing of Precalculated Vibrational Scaling Factors*, 2022)	M05-2X 6-311 (d) G+ 0.9483(Sutton et al., 2015)	M06-2X 6-311 (d)G+ 0.9567 (Ünal et al., 2021)	
ν_1	ν CH (80%) in C10-H11 + ν CH (15%) in C8-H9	3017 m	3028 m	3026 m	3014 m
ν_2	ν_{asym}CH(100%) in CH3	2933 w	2954 w	2963 w	2919 w
ν_3	ν_{sym}CH (83%) in CH3	2897 w	2911 w	2911 w	2850 w
ν_4	ν_{sym} C=C (56%) in C8-C10 + ν_{asym} CC (10%) in C6-C4	1653 m	1670 m	1679 m	1648 m
ν_5	ν_{asym} C=C (64%) in C6-C4 + ν_{sym} CC (10%) in C8-C10	1616 m	1628 m	1638 m	1618 s
ν_6	ν_{asym}(85%) in O3-C1-O2	1505 s	1534 s	1562 s	1555 s
ν_7	β_{asym} HCH (90%) in CH3	1445 m	1438m	1435 m	1435 m
ν_8	ν_{sym}(72%) in O3-C1-O2	1354 s	1387 s	1398 s	1387 s
ν_9	β_{asym} HCC (46%) in H5-C4-C1 + β CCC(18%) in C6-C8-C10	1269 m	1259 m	1259 m	1277 m
ν_{10}	β_{asym} HCC (79%) in H5-C4-C1	1237 w	1244 w	1233 w	1208 w
ν_{11}	ν C-C (51%) in C6-C8 + β CCC (13%) in C6-C8-C10+β_{asym} HCC (10%) in H5-C4-C1	1181 w	1192 w	1186 w	1148 w
ν_{12}	τ HCCO (86%) in H5-C4-C1-O2	1039 s	1056 s	1052 s	1006 s
ν_{13}	β_{asym}HCC (12%) in H5-C4-C1 + ν CC (53%) in C1-C4 + τ HCCC (10%) in H14-C12-C10-C8	978 m	1000 m	997 m	962 m
ν_{14}	ν CC (28%) in C10-C12 +τ HCCC (26%) in H14-C12-C10-C8 + ν CC (16%) in C4-C1	938 vw	948 w	941 w	952 w
ν_{15}	τ HCCO (60%) in H5-C4-C1-C2 + γ COOC (16%) in C4-O2-O3-C1	919 vw	940 m	937m	884 m
ν_{16}	τ HCCC (54%) in H11-C10-C8-C6 + τ HCCC (11%) in H13-C12-C10-C8 + γ COOC (22%) in C4-O2-O3-C1	831 vw	849 w	845 w	808 w
ν_{17}	τ HCCC (17%) in H11-C10-C8-C6 + τ CCCC (10%) in C1-C4-C6-C8	734 w	748 w	745 w	734 w
ν_{18}	β OCO (71%) in O2-C1-O3 + γ COOC (48%) in C4-O2-O3-C1	733 m	752 m	751 m	708 m
ν_{19}	β CCO (68%) in C4-C1-O3	588 m	594 m	592 m	577 m

ν: stretching; β: in-plane bending;γ: out-of-plane bending;τ : torsion; as—asymmetric, sym—symmetric s: strong; m:medium; w: weak; vw: very weak, [*]Potential energy distribution (PED), less than 10%are not shown.

Since, the vibrational frequencies were calculated in the gas phase and the experimental values were obtained in solid phase, a difference was noticed between the theoretical and experimental frequencies, more precisely at high frequencies (above 1500 cm^{-1}). The high theoretical frequencies were therefore multiplied by a scaling factor to better fit the experimental results, this method has been frequently used by several researchers namelyJamrózet *al*(Jamróz & Dobrowolski, 2001),Kose(Kose, 2016)andSert et *al*(Sert et al., 2015),(Sert, Singer, et al., 2014). The experimental FT-IR spectrum of the potassium sorbate was compared to the theoretical spectra and represented in Figure 2, Figure 3 and Figure 4 as well as the correlation graph that describes the agreement between the computed and experimental wavenumbers.

The resulting calculated and experimental wavenumber relationships are linearly related, the relationships are expressed by the following equation:

$$v_{Cal} = 1.00043 \, v_{exp} - 8.59377 \textit{ for B3LYP-D3 method}$$

$$v_{Cal} = 0.83242 \, v_{exp} - 211.1698 \textit{ for M05-2X method}$$

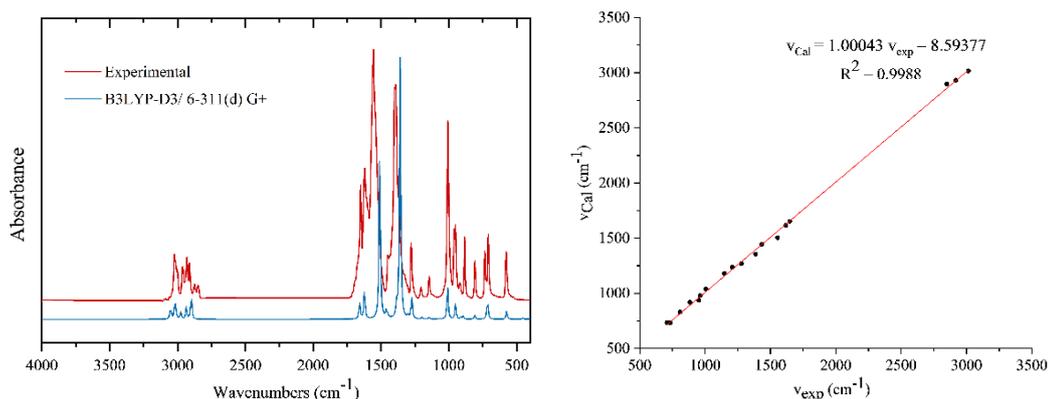$$v_{Cal} = 1.00409 \, v_{exp} - 18.7901 \textit{ for M06-2X method}$$

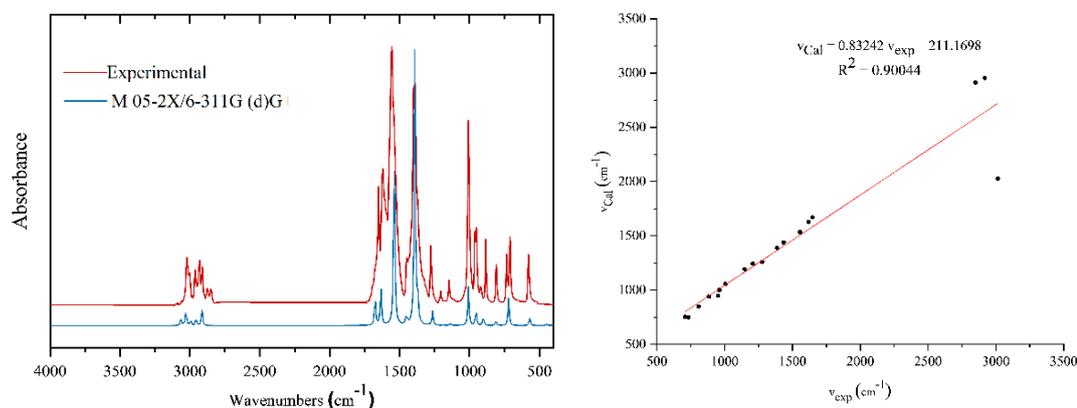Figure 1. Comparison between experimental and computed vibrations with B3LYP-D3/6-311(d)G+

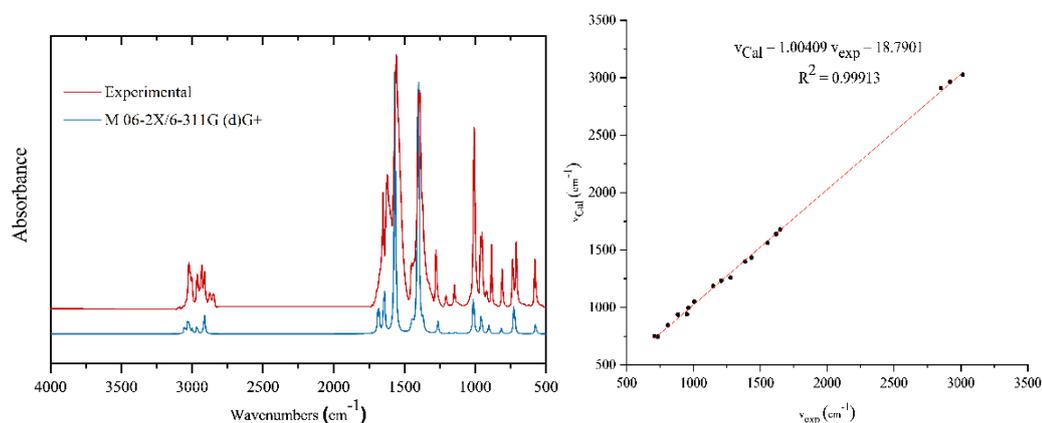Figure 3. Comparison between experimental and computed vibrations with M05-2X/6-311(d)G+

Figure 4. Comparison between experimental and computed vibrations with M06-2X/6-311(d)G+

The coefficient of correlation R^2 values (R^2 = 0.9988 for *B3LYP-D3*), (R^2 = 0.90044 for *M05-2X*) and (R^2 = 0.99913 for *M06-2X*) between the computed and experimental wavenumbers values. As it can be clearly seen, the calculated data describean excellent correlation with the corresponding experimental data when using *M06-2X*functional.

UV-vis Spectral Analysis

The electronic spectrum of potassium sorbate in water shows a strong peak at 254 nm, corresponding to one transition from the ground state of the sorbate molecule to an excited state. The time-dependent density functional theory (TD-DFT (Hamrani et al., 2021)) calculations were conducted at *M06-2X/6-311(d) G + level*, in order to identify the number and contributions of the molecular orbitals involved in the electronic transitions, the theoretical data were extracted using the Gauss-Sum 2.2 program (Halim & Ibrahim, 2021a) and tabulated in Table 3. It worth noting that the solute electron density solvation model (SMD (Sutton et al., 2015)) was applied in the calculations considering possible interactions between the solvent molecules and the sorbate anion, that affect the electronic spectrum.
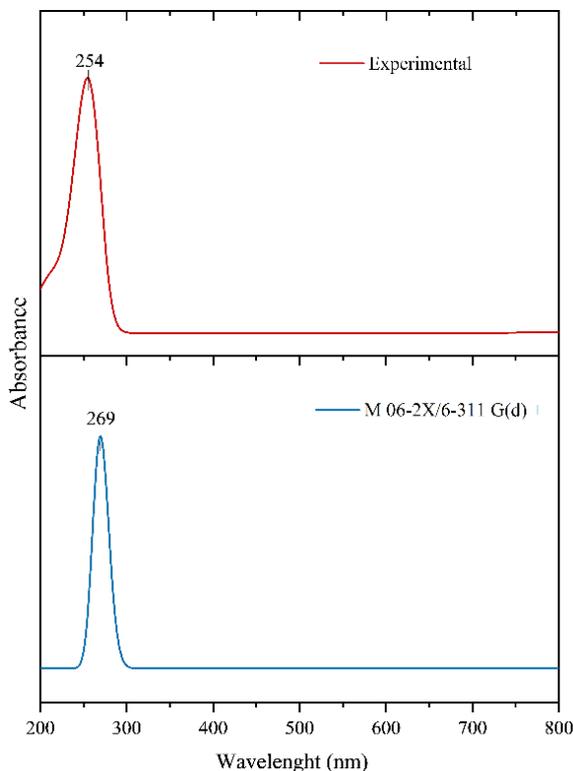

Figure 5. Comparison between experimental and calculated UV-Vis spectra

Table3. Experimental and computed spectroscopic parameter of sorbate anion.

Observed Transition	Observed λ_{max} (nm)	Calculated λ_{max} (nm)	Oscillatory Strength f (a.u)	No.OM	Contributing Molecular orbital (%)
1	254	269	0.9319	30,31	HOMO → LUMO (97%)
2	--	271	0.0001	28,31	HOMO – 2 → LUMO (98%)
3	--	302	0.0	29,31	HOMO – 1 → LUMO (97%)

The TD-DFT calculations are in a good agreement with the experimentaldata, by anticipating an intense electronic transition at 269 nm with an oscillator strength *f* = 0.9319 nearly equal to 1. Two more transitions were predicted, with oscillator strength values close to zero indicating low intensities, which explains their non-apparitions in the electronic spectrum.

The molecular orbitals contributing in the electronic transitions (HOMO) and (LUMO), as well as (HOMO – 1) and (HOMO – 2) along with their calculated energies were representing in Figure 6, where the positive zone is red and the negative zone is green (Halim & Ibrahim, 2021a).

From Figure 6, it can be seen that the HOMO which represents the highest occupied molecular orbital, was mainly situated on the π-bonding of the two oxygens contained in the carboxyl moiety, as well as on the π-bonding of the double bound carbons. Whereas, the LUMO which represents the highest excited state has an electron density mainly localized on the two oxygens of the carboxyl group, identified by π*-antibonding of C1-O3, C1-O2 bonds. This brief analysis suggests that the observed transition on the UV-Vis spectrum may corresponds to the transitionfrom the π-bonding of the HOMO to the π*-anti-bonding of the LUMO, an NBO analysis must be done to confirm that.
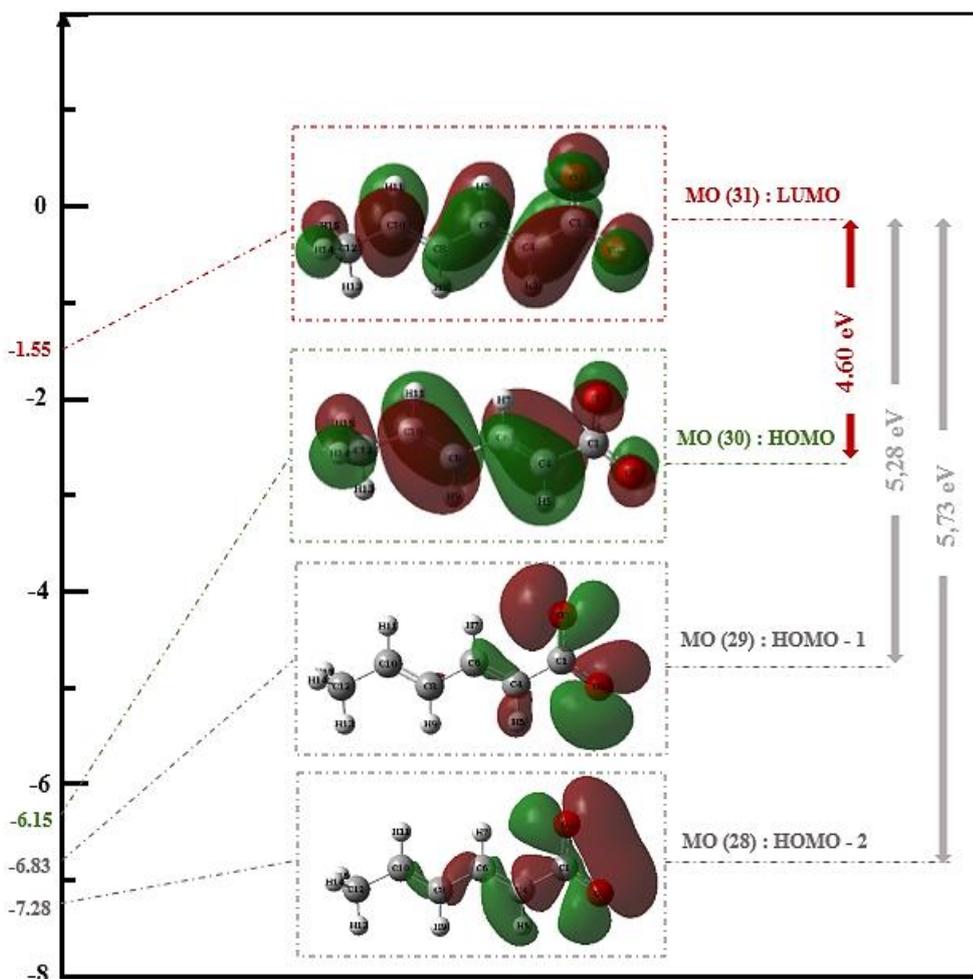
Figure 6. 3D plot molecular orbitals and their energies of transition

Natural Bond Orbital (NBO) Analysis

NBO analysis was conducted at *M06-2X /6-311(d) G+*in order to confirm the nature of observed transitions in the theoretical UV-Vis Spectrum. NBO analysis is based on the electron density delocalization from the occupied Lewis-type (donor) natural bond orbitals to unoccupied non-Lewis-type (acceptor) natural bond orbitals.According to the second order Fock matrix in NBO analysis(Devi et al., 2018),the correlation between donor (i),acceptor (j) level bonds and stabilization energy E (2) [donor (*i*) → acceptor (*j*)] is expressed as follows (Devi et al., 2018):

$$E(2) = \text{Delta } E_{ij} = qi \frac{(F_{ij})^2}{(E_j - E_i)} \dots (1)(\text{Devi et al., 2018})$$

Where, *qi*: occupancy of donor orbital; E_i and E_j: diagonal elements; F_{ij}: off diagonal NBO Fock matrix element. In here, several donor/acceptor interactions were identified for the sorbate anion. The major intramolecular transitions and their stabilization energies E (2)are tabulated in descending order in Table 4.

According to the literature, the higher stabilization energy E (2)value, more intense is the interaction between electron donors and acceptors (Devi et al., 2018; Kerru et al., 2019).The highest stabilization energy for sorbate anion was noticed for the intramolecular transition the **π** (C4 – C6) bond to the **π*** (C8 – C10) anti-bonds with stabilization energy 19.80 Kcal mol^{-1}, which indicate the probable intramolecular interaction in HOMO-LUMO transition. Thus, the suggestion proposed using UV-Vis analysis were successfully confirmed.

Other intramolecular charge transfers happen from A charge transfer is also seen from π (C 8 - C 10) to π* (C4 – C6) and with stabilization energy 12.85 Kcal mol^{-1}. It worth noting that lower stabilization energies were observed with 5.59, 5.29 and 5.27 Kcal/mol, corresponding to transitions from σ (C10 – H 11), σ (C8 - H 9) and σ (C6 - H7) bonds to σ* (C8 - H9), σ* (C10 - H11) and σ* (C4 - H 5) bonds, respectively.

Table 4. Experimental and computed spectroscopic parameter values of sorbate anion.

Donor (i)	Type	Acceptor (j)	Type	E (2)(Kcal/mol)	E(j) - E(i) (a.u)	F(i.j) (a.u)
C 4 – C6	π	C 8 - C 10	π^*	19.80	0.28	0.066
O2	n	C 1 - O3	π^*	19.77	0.71	0.107
O3	n	C1 - C 4	π^*	15.60	0.60	0.087
O2	n	C 1 – C4	π^*	13.85	0.61	0.082
C 4 - C 6	π	C 1 - O 2	π^*	13.00	0.29	0.060
C 8 - C 10	π	C4-C6	π^*	12.85	0.34	0.059
C 1 - O 2	π	C4-C6	π^*	6.80	0.33	0.043
C 10 – H 11	σ	C 8 - H 9	σ^*	5.59	0.93	0.064
C 8 - H 9	σ	C 10 - H 11	σ^*	5.29	0.92	0.062
C 6 - H 7	σ	C 4 - H 5	σ^*	5.27	0.93	0.063
C 1 - C 4	σ	C 6 - C 8	σ^*	4.68	1.09	0.064
C 6 - H 7	σ	C 8 - H 9	σ^*	3.92	0.89	0.053
C 6 - C 8	σ	C 10 - C 12	σ^*	3.84	1.05	0.057
C 12 - H 13	σ	C 10 - H 11	σ^*	3.77	0.93	0.053
C 10 - C 12	σ	C 6 - C 8	σ^*	3.63	1.16	0.058

n :lone pair or nonbonding orbital ; π : pi-bonding orbital ; σ: sigma- bonding orbital ; π^*: pi-antibonding orbital ; σ^* :sigma-antibonding orbital

Molecular Electrostatic Potential (MEP) Analysis

One of the most interesting characteristics of quantum chemistry is the capacity to anticipate the reactive sites in the moleculeusing theMEPsurface (Devi et al., 2018), which plot the charge distribution of the molecules in three dimensions (Devi et al., 2018), this charge can be used to determine electrophilic, nucleophilic sites (Devi et al., 2018). In the MEP map, the potential varies between -0.256 a.u and 0.256 a.u and enhance in the order of red < orange < yellow < green < blue (Devi et al., 2018), (Halim & Ibrahim, 2021b), where blue indicates the most attractive sites and red the most repulsive sites (Halim & Ibrahim, 2021b). In another words, the red region (negative electrostatic potential) represents the electrophilic attack, while the blue region (positive electrostatic potential) represents the nucleophilic attack (Halim & Ibrahim, 2021b).For the sorbate anion, molecular electrostatic potential (MEP) 3D surfaces were obtained at *M06-2X/6-311 (d) G+* level and represented in Figure 7.
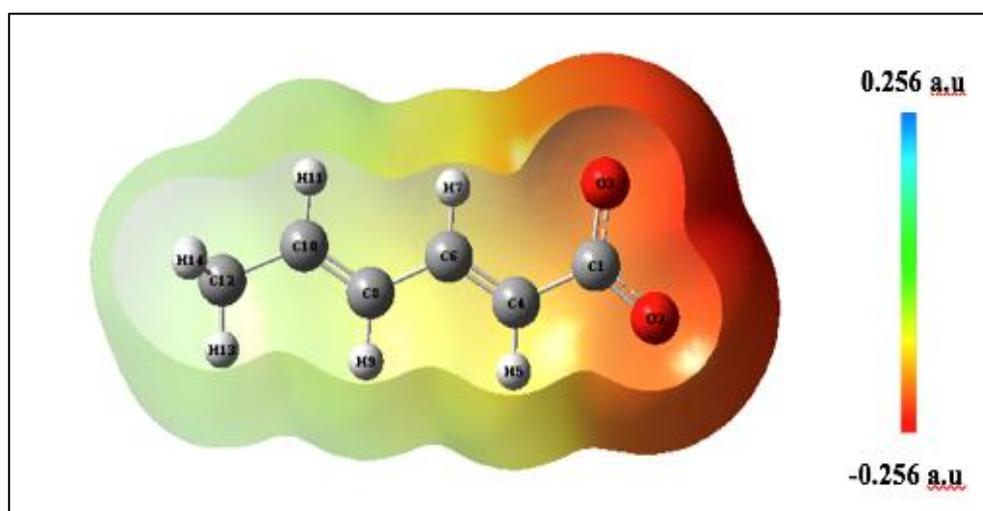

Figure 7. MEP map of the optimized structure of sorbate anion

The red region located on the oxygen atoms O2 and O3 representsthe mostnegative electrostatic potentialregion with the following values -0.216 à -0.23 a.u. Thus, the oxygens O2 and O3 having the strongest repulsion and are the most expected sites to be attacked. Additionally, the negative orange and yellowregions (C 8 - C 10) and (C4 – C6) are related to electrophilic reactivity(Halim & Ibrahim, 2021b). These investigations are useful to provide information about the reactivity of the molecule for further studies.

Global Reactivity Descriptors (GRDs)

GRDs such as ionization potential (IP), electron affinity (EA)electronegativity (χ), chemical potential (μ), chemical hardness (η) and the electrophilicity index (ω)(Saravanamoorthy et al., 2021) ,areimportant for the reactivity investigation of molecular systems (Zaater et al., 2016). These parameters can be calculated from the HOMO- LUMO orbitals values acoording to Parr and Pearson(Parr & Pearson, 1983) and employing the following equations (1-6) given in ref (Devi et al., 2018), (Pearson, 1986), (Yang & Parr, 1985). The global reactivity descriptors of potassium sorbate were calculated, and their values were summarized in Table 5.

$$IP = -E_{HOMO} \cdots (1)$$

$$EA = -E_{LUMO} \cdots (2)$$

$$\chi = -\frac{1}{2}(E_{LUMO} + E_{HOMO}) \cdots (3)$$

$$\mu = -\chi = \frac{1}{2}(E_{LUMO} + E_{HOMO}) \cdots (4)$$

$$\eta = \frac{1}{2}(E_{LUMO} - E_{HOMO}) \cdots (5)$$

$$s = \frac{1}{2\eta} \cdots (6)$$

$$\omega = \frac{\mu^2}{2\eta} \cdots (7)$$

Table 5 .Global reactivity descriptors of the optimized structure of potassium sorbate

Global reactivity descriptors	Values (eV)
HOMO–LUMO band gap (E gap)	4.60
HOMO energy (E_{HOMO})	-6.15
LUMO energy (E_{LUMO})	-1.55
Ionization potential (IP)	6.15
Electron affinity (EA)	1.55
Electronegativity (χ)	2.3
Chemical potential (μ)	-2.3
Chemical hardness (η)	2.3
Chemical softness (s)	0.23
Electrophilicity index (ω)	1.15

As mentioned in Figure 6, the HOMO and LUMO are predicted to be equal to -6.15 eV and -1.55 eV, respectively. The difference HOMO-LUMO energy gap (Egap) is equal to 4.60 eV directly related to the chemical reactivity of the molecule (Sert, Balakit, et al., 2014); It reflects the capacity for charge transfer interactions to occur within the molecule(Nemes et al., 2020), In the literature, a low band gap energy (< 5 eV) suggests a high chemical reactivity (Saravanamoorthy et al., 2021), which is often responsible of the bioactivity of molecules, since it facilitated the charge transfers between the molecules and the proteins (Zaater et al., 2016).

The ionization energy value implies that an energy value of 6.15 eV is needed to withdraw an electron from the HOMO (Fathima Rizwana et al., 2019). In another hand, the lower value of electron affinity (1.55 eV) displays that the moleculecan easily accept electrons, these values are also reflecting the biological activity of the title compound (Ait Ramdane et al., 2021).

Structure–Activity Relationship

Molecular Docking

Enolase is a glycolytic metalloenzym implicated in carbon metabolism. The interest in targeting enolase is in its essential role in a number of biological processes, such as cell wall formation and RNA synthesis, as well as its role as a plasma cell receptor, Validating the antibacterial potential of candidate molecule is done by examining carefully the position and character of chelating moieties for stronger interaction with metal ions and enolase active site residues (Krucinska et al., 2019).
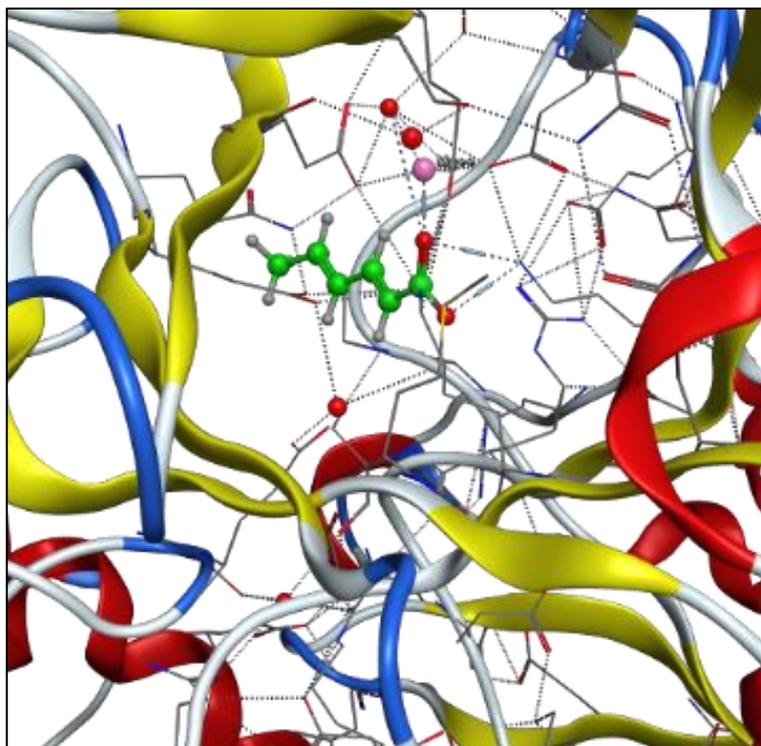
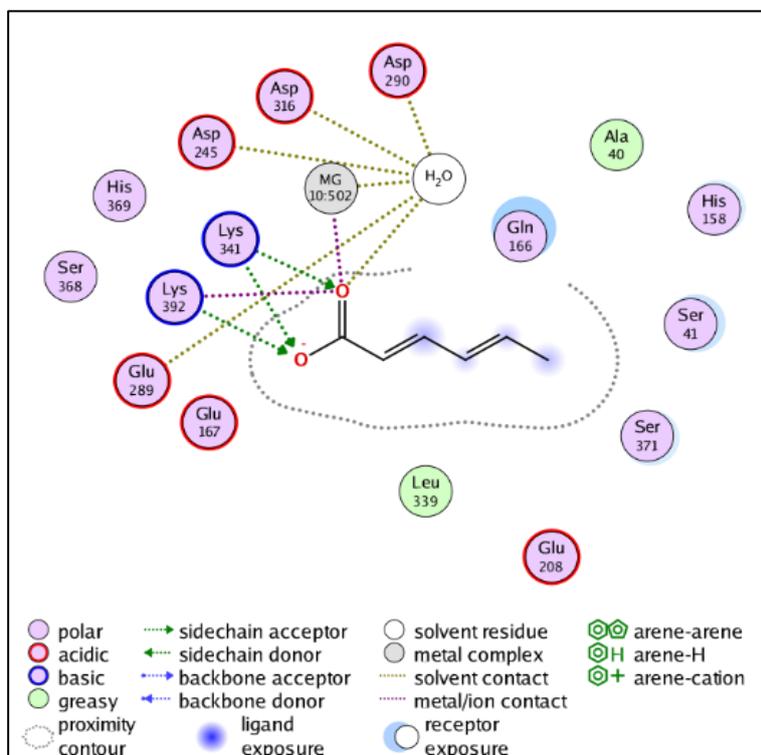Figure 8. 3D representation of the best binding pose

Figure 9. 2D representation of the best binding pose

The docking of sorbate anion in the active site of enolase (Figure 8 and 9) shows that the molecule interacts with Mg(II) cation through an electrostatic interaction. It also interacts with the residues Lys341 and Lys391, and with Asp245, Asp316 and Asp 290 through H_2O. These numerous interactions explained the quite high value of the binding energy (6.3 Kcal/mol). The results displayed clearly that the carboxylate group in the sorbate anion molecule is the one that interacts in the binding site of enolase, as supported by previous theoretical calculations this group is the more chemically reactive, and molecular docking analysis proved in here that this group is responsible for the biological activity of sorbate.

In Silico ADME Analysis

The most popular method used for defining the drug-likeness is the prediction of six physicochemical properties like lipophilicity, size, hydrogen-bonding etc. In here, those parameters were conducted using SwissADME server and summarized in Table 6.

Table 6. Physicochemical descriptors predicted by SwissADME server

Physicochemical property	Physicochemical descriptors	Sorbate anion
Lipophilicity	Log P	0.86
	H-bond donors	0
Hydrogen bonds	H-bond acceptors	2
Molecular weight	MW (g.mol^{-1})	111.12
Flexibility	Rotatable bonds	2
Polarity	TPSA (Å^2)	40.13
Solubility	Log S	-1.23
Saturation	Fraction of C sp^3	0.17

According to Lipinski's rule of five, the compounds with a logP (octanol–water partition coefficient) $\leq$ 5 possesses a good lipophilicity, which induce a significant permeability in the cellular plasma membrane (Turner & Agatonovic-Kustrin, 2007), (Winiwarter et al., 2007). In here sorbate anion has a low lipophilicity, as seen from Table 6, attesting of a good cell permeability favoring the permeation through the lipoid layers of the bacterial membranes (Riswan Ahamed et al., 2014).

The existence of many hydrogen bonds can increase diffusion of a drug across cell membranes, and further, the ability to establish important interactions with the protein targets (Coimbra et al., 2020), In the other hand, too many hydrogen bond donors/acceptors can cause a decrease of the affinity toward the lipid membrane (Coimbra et al., 2020), In that regard, the rule of five attests that a number of hydrogen bond donor lower than five and hydrogen bond acceptors (N and O atoms) lower than 10 are favorable for a good bioavailable molecule(Winiwarter et al., 2007), which is the case of the sorbate anion.

Molecular weight is widely applied to separate molecules with important bioavailability from those with less. In fact, compounds with molecular weight greater than 500 g.mol^{-1} are considered as poor bioavailable. However, there are recent reports suggesting that compounds with a molecular weight higher than 500 g.mol^{-1} and meet the two criteria of : (1) ten or fewer rotatable bonds (flexibility) and (2) topologic polar surface area (TPSA) equal to or less than 140 (Å^2) will have a high probability of good bioavailability (Df et al., 2002), In our case, it is clear that the sorbate anion tends to fulfil those two criteria, despite its low molecular weight (111.12 g.mol^{-1}).

Sufficient aqueous solubility is an essential requirement for small molecule to interfere the bacterial cell , and improving the aqueous solubility of bioactive compounds is often a major problem for medicinal chemists(Ishikawa, 2022).Fortunately, the sorbate anion possesses a high solubility (-6 $\leq$Log S (Daina et al., 2017)). Figure 9 represents the bioavailability radar generated by SwissADME, it can be clearly seen that the sorbate anionis in the optimum range of bioavailable molecule (red area).
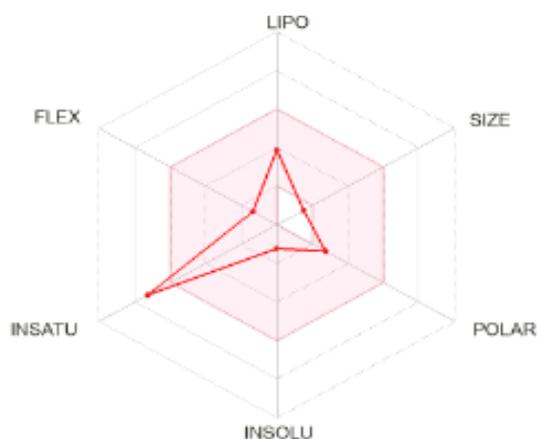

Figure 9. Bioavailability radar of sorbate provided by SwissADME

Conclusion

In this investigation, the geometry of the potassium sorbate was optimized with three functionals:*B3LYP-D3*, *M05-2X* and *M06-2X* using *6-311 (d) G+* basis set. The theoretical results were compared to the corresponding experimental results and a considerable level of correlation has been noticed when using DFT/M06-2X with 6-311+G(d) basis set (R^2 = 0.99913).TD-DFT approach was conducted on the optimized structure of the sorbate anion, in order to explore its probable electronic transitions, UV-vis spectrum showed one transition at 269 nm, which matched perfectly with the experimental spectrum and corresponded to the transition of electrons from HOMO to LUMO orbitals. According NBO analysis, the π-orbitals and π*- orbitals contained in HOMO and LUMO molecular orbitals are in the origin of the transition observed in UV-Vis spectrum. Molecular electrostatic potential (MEP) revealed that electrophilic sites are found around the oxygen atoms of the carboxylate moiety in the sorbate anion. The HOMO, LUMO and HOMO-LUMO gap values were -6.15 eV, -1.55 eV and 4.60 eV, respectively, and the global reactivity descriptors (GRDs) demonstrated that the charge is transferred easily within the sorbate molecule, which confirmed again its high reactivity. Molecular docking of sorbate anion supports the fact that the expected reactive group i.e., carboxylate group is responsible of the biological activity of sorbate, by interacting with Mg(II) and amino- acids residues of Enolase enzyme. The computational ADME properties were predicted and summarized via the SwissADME computational tool and the results were supporting the structure-activity relationship of the sorbate anion for the aspect of antibacterial activity.

Recommendations

The findings of this study revealed the structure-activity relationship between the structure of sorbate anion and its biological activity, and will greatly help for further investigation on the sorbate molecule.

Scientific Ethics Declaration

The authors declare that the scientific ethical and legal responsibility of this article published in EPSTEM journal belongs to the authors.

Acknowledgements or Notes

*This article was presented as a poster presentation at the International Conference on Research in Engineering, Technology and Science (www.icrets.net) held in Budapest/Hungary on July 06-09, 2023.

References

Ait Ramdane, K., Terbouche, A., Ait Ramdane-Terbouche, C., Lakhdari, H., Bachari, K., Merazig, H., Roisnel, T., Hauchard, D., & Mezaoui, D. (2021). Crystal structure, characterization and chemical reactivity of novel piperazine derivative ligand for electrochemical recognition of nitrite anion. *Journal of Chemical Sciences*, *133*(1), 18.

Alghamdi, A. A., Alam, M. M., & Nazreen, S. (2020). In silico ADME predictions and in vitro antibacterial evaluation of 2-hydroxy benzothiazole-based 1,3,4-oxadiazole derivatives. *Turkish Journal of Chemistry*, *44*(4), 1068–1084.

Alomari, A. (2018). *Biophysical and kinetic analysis of escherichia coli DNA ligase activity and inhibition*. (Doctoral dissertation, University of Portsmouth).

Angelova, V. T., Valcheva, V., Pencheva, T., Voynikov, Y., Vassilev, N., Mihaylova, R., Momekov, G., & Shivachev, B. (2017). Synthesis, antimycobacterial activity and docking study of 2-aroyl-[1]benzopyrano[4,3-c]pyrazol-4(1H)-one derivatives and related hydrazide-hydrazones. *Bioorganic & Medicinal Chemistry Letters*, *27*(13), 2996–3002.

Baldevraj, R. S. M., & Jagadish, R. S. (2011). 14—Incorporation of chemical antimicrobial agents into polymeric films for food packaging. In J.-M. Lagarón (Ed.), *Multifunctional and Nanoreinforced Polymers for Food Packaging* (pp. 368–420). Woodhead Publishing.

Bank, R. P. D. (1971). *RCSB PDB - 6BFZ: Crystal structure of enolase from E. coli with a mixture of apo form, substrate, and product form*. Retrieved June 29, 2023, from https://www.rcsb.org/structure/6BFZ

CCCBDB listing of precalculated vibrational scaling factors. (2022). Retrieved October 10, 2021, from https://cccbdb.nist.gov/vibscalejust.asp

Chahardoli, A., Jalilian, F., Memariani, Z., Farzaei, M. H., & Shokoohinia, Y. (2020). Chapter 26—Analysis of organic acids. In A. Sanches Silva, S. F. Nabavi, M. Saeedi, & S. M. Nabavi (Eds.), *Recent Advances in Natural Products Analysis* (pp. 767–823). Elsevier.

Chemical Computing Group, Montreal, Canada. (2015). *Molecular Operating Environment (MOE)*. http://www.chemcomp.com

Coimbra, J. T. S., Feghali, R., Ribeiro, R. P., Ramos, M. J., & Fernandes, P. A. (2020). The importance of intramolecular hydrogen bonds on the translocation of the small drug piracetam through a lipid bilayer. *RSC Advances*, *11*(2), 899–908.

Daina, A., Michielin, O., & Zoete, V. (2017). SwissADME: A free web tool to evaluate pharmacokinetics, drug-likeness and medicinal chemistry friendliness of small molecules. *Scientific Reports*, *7*(1), Article 1.

Davidson, P. M. (2005). *Antimicrobials in food* (3rd ed.). Taylor & Francis Group,.

Devi, P., Fatma, S., Bishnoi, A., Srivastava, K., Shukla, S., & Kumar, R. (2018). Synthesis, spectroscopic and DFT studies of novel 4-(morpholinomethyl)-5-oxo-1-phenylpyrrolidine-3-carboxylic acid. *Journal of Molecular Structure*, *1157*, 551–559.

Df, V., Sr, J., Hy, C., Br, S., Kw, W., & Kd, K. (2002). Molecular properties that influence the oral bioavailability of drug candidates. *Journal of Medicinal Chemistry*, *45*(12).

Dimić, D., Milenković, D., Ilić, J., Šmit, B., Amić, A., Marković, Z., & Dimitrić Marković, J. (2018). Experimental and theoretical elucidation of structural and antioxidant properties of vanillylmandelic acid and its carboxylate anion. *Spectrochimica Acta Part A: Molecular and Biomolecular Spectroscopy*, *198*, 61–70.

D'Souza, M. J., Koyoshi, F., & Everett, L. M. (2009). Structure activity relationships (SARs) using a structurally diverse drug database: Validating success of predictor tools. *Pharmaceutical Reviews*, *7*(5), https://web.archive.org/web/20100125114948/http://www.pharmainfo.net/reviews/structure-activity-relationships-sars-using-structurally-diverse-drug-database-validating-su.

Fathima Rizwana, B., Christian Prasana, J., Muthu, S., & Susan Abraham, C. (2019). Spectroscopic (FT-IR, FT-Raman, NMR) investigation on 2-[(2-amino-6-oxo-6,9-dihydro-3H-purin-9-yl)methoxy]ethyl(2S)-2-amino-3-methylbutanoate by density functional theory. *Materials Today: Proceedings*, *18*, 1770–1782.

Grimme, S., Ehrlich, S., & Goerigk, L. (2011). Effect of the damping function in dispersion corrected density functional theory. *Journal of Computational Chemistry*, *32*(7), 1456–1465.

Guerrero-Perilla, C., Bernal, F. A., & Coy-Barrera, E. D. (2015). Molecular docking study of naturallyoccurring compounds as inhibitors of N-myristoyl transferase towards antifungal agents discovery. *Revista Colombiana de Ciencias Químico Farmacéuticas*, *44*(2), 162–178.

Halim, S. A., & Ibrahim, M. A. (2021a). Synthesis, FT-IR, structural, thermochemical, electronic absorption spectral, and NLO analysis of the novel 10-methoxy-10 *H* -furo[3,2- *g*]chromeno[2,3- *b*][1,3]thiazolo[5,4- *e*]pyridine-2,10(3 *H*)-dione (MFCTP): A DFT/TD-DFT study. *RSC Advances*, *11*(51), 32047–32066.

Halim, S. A., & Ibrahim, M. A. (2021b). Synthesis, FT-IR, structural, thermochemical, electronic absorption spectral, and NLO analysis of the novel 10-methoxy-10 *H* -furo[3,2- *g*]chromeno[2,3- *b*][1,3]thiazolo[5,4- *e*]pyridine-2,10(3 *H*)-dione (MFCTP): A DFT/TD-DFT study. *RSC Advances*, *11*(51), 32047–32066.

Hamrani, O., Amina, Z., Boutamine, S., Taïri-Kellou, S., & Hank, Z. (2021). Structure-properties relationship of Cu (II) – paracetamol based complex. density functional theory and spectroscopic studies. *Novel Approaches in Drug Designing & Development, 5*(4), 555667.

Ishikawa, M. (2022). [Improvement in aqueous solubility of bioactive molecules by decreasing intermolecular interaction]. *Yakugaku Zasshi: Journal of the Pharmaceutical Society of Japan*, *142*(4), 365–379.

James, H. (2022). Structural activity relationship of drugs and its applications. *Journal of Pharmacological Reports*, *6*(2), 1–1.

Jamróz, M. H., & Dobrowolski, J. Cz. (2001). Potential energy distribution (PED) analysis of DFT calculated IR spectra of the most stable Li, Na, and Cu(I) diformate molecules. *Journal of Molecular Structure*, *565–566*, 475–480.

Kalhotra, P., Chittepu, V. C. S. R., Osorio-Revilla, G., & Gallardo-Velázquez, T. (2018). Structure–activity relationship and molecular docking of natural product library reveal chrysin as a novel dipeptidyl peptidase-4 (dpp-4) inhibitor: An integrated in silico and in vitro study. *Molecules*, *23*(6), Article 6.

Kerru, N., Gummidi, L., Bhaskaruni, S. V. H. S., Maddila, S. N., Singh, P., & Jonnalagadda, S. B. (2019). A comparison between observed and DFT calculations on structure of 5-(4-chlorophenyl)-2-amino-1,3,4-thiadiazole. *Scientific Reports*, *9*(1), 19280.

Kleeb, S. (2015). *Crystal structure of FimH in complex with 3'-Chloro-4'-(alpha-D-mannopyranosyloxy)-biphenyl-4-carbonitrile*. Retrieved September 20, 2022, from https://www.rcsb.org/structure/4CST

Kose, E. (2016). The spectroscopic analysis of 2,4'-dibromoacetophenone moleculeby using quantum chemical calculations. *Anadolu University Journal of Science and Technology A - Applied Sciences and Engineering*, *17*(AFG5 SPECIAL ISSUE), 677–677.

Krucinska, J., Falcone, E., Erlandsen, H., Hazeen, A., Lombardo, M. N., Estrada, A., Robinson, V. L., Anderson, A. C., & Wright, D. L. (2019). Structural and functional studies of bacterial enolase, a potential target against gram-negative pathogens. *Biochemistry*, *58*(9), 1188–1197.

Liang, M., Hada, M., Ehara, K., Toyota, R., Fukuda, J., Hasegawa, M., Ishida, T., Nakajima, Y., Honda, O., Kitao, H., Nakai, T., Vreven, K., Throssell, J. A., Montgomery, Jr., J. E., Peralta, F., Ogliaro, M., Bearpark, J. J., Heyd, E., Brothers, K. N., Kudin, V. N., Staroverov, T., Keith, R., Kobayashi, J., Normand, K., Raghavachari, A., Rendell, J. C., Burant, S. S., Iyengar, J., Tomasi, M., Cossi, J. M., Millam, M., Klene, C., Adamo, R., Cammi, J. W., Ochterski, R. L., Martin, K., Morokuma, O., Farkas, J. B., Foresman, D. J., & Wallingford CT. (2009). *Gaussian 09* (Revision A.02) Gaussian, Inc., [Computer software].

Mackowiak-Dryka, M., Paszkiewicz, W., & Drozd, L. (2015). Parabens: Food preservatives and consumer safety. *Medycyna Weterynaryjna*, *71*, 553–556.

Mehandzhiyski, A. Y., Riccardi, E., van Erp, T. S., Koch, H., Åstrand, P.-O., Trinh, T. T., & Grimes, B. A. (2015). Density functional theory study on the interactions of metal ions with long chain deprotonated carboxylic acids. *The Journal of Physical Chemistry A*, *119*(40), 10195–10203.

Mehta, N., & Goerigk, L. (2021). Assessing the applicability of the geometric counterpoise correction in B2PLYP/Double-ζ calculations for thermochemistry, kinetics, and noncovalent interactions*. *Australian Journal of Chemistry*.

Nemes, D., Kovács, R., Nagy, F., Tóth, Z., Herczegh, P., Borbás, A., Kelemen, V., Pfliegler, W. P., Rebenku, I., Hajdu, P. B., Fehér, P., Ujhelyi, Z., Fenyvesi, F., Váradi, J., Vecsernyés, M., & Bácskay, I. (2020). Comparative biocompatibility and antimicrobial studies of sorbic acid derivates. *European Journal of Pharmaceutical Sciences*, *143*, 105162.

Parr, R. G., & Pearson, R. G. (1983). Absolute hardness: Companion parameter to absolute electronegativity. *Journal of the American Chemical Society*, *105*(26), 7512–7516.

Pearson, R. G. (1986). Absolute electronegativity and hardness correlated with molecular orbital theory. *Proceedings of the National Academy of Sciences*, *83*(22), 8440–8441.

Piper, P. W. (2018). Potential Safety Issues Surrounding the Use of Benzoate Preservatives. *Beverages*, *4*(2).

Reichle, D. E. (2020). Chapter 2—The physical and chemical bases of energy. In D. E. Reichle (Ed.), *The Global Carbon Cycle and Climate Change* (pp. 5–14). Elsevier.

Riswan Ahamed, M. A., Azarudeen, R. S., & Kani, N. M. (2014). Antimicrobial applications of transition metal complexes of benzothiazole based terpolymer: Synthesis, characterization, and effect on bacterial and fungal strains. *Bioinorganic Chemistry and Applications*, *2014*, 1–16.

Salami, N., & Shokri, A. (2021). Chapter 5—Electronic structure of solids and molecules. In M. Ghaedi (Ed.), *Interface Science and Technology, 32,* 325–373. Elsevier.

Santiesteban-López, N. A., Rosales, M., Palou, E., & López-Malo, A. (2009). Growth response of escherichia coli ATCC 35218 adapted to several concentrations of sodium benzoate and potassium sorbate. *Journal of Food Protection*, *72*(11), 2301–2307.

Saravanamoorthy, S. N., Vasanthi, B., & Poornima, R. (2021). *Molecular geometry, vibrational spectroscopic, molecular orbital and Mulliken charge analysis of 4-(carboxyamino)-benzoic acid: Molecular docking and DFT calculations*. file:///C:/Users/pc/Downloads/preprints202107.0215.v1.pdf

Savjani, K. T., Gajjar, A. K., & Savjani, J. K. (2012). Drug solubility: Importance and enhancement techniques. *ISRN Pharmaceutics*, *2012*, 195727.

Schlitter, S. M., & Beck, H. P. (1996). Crystal structure, solid-state polymerization, and ionic conductivity of alkali salts of unsaturated carboxylic acids, 4. investigations on lithium sorbate. *Chemische Berichte*, *129*(12), 1561–1564.

Sert, Y., Balakit, A. A., Öztürk, N., Ucun, F., & El-Hiti, G. A. (2014). Experimental (FT-IR, NMR and UV) and theoretical (M06-2X and DFT) investigation, and frequency estimation analyses on (E)-3-(4-bromo-5-methylthiophen-2-yl)acrylonitrile. *Spectrochimica Acta Part A: Molecular and Biomolecular Spectroscopy*, *131*, 502–511.

Sert, Y., Puttaraju, K. B., Keskinoğlu, S., Shivashankar, K., & Ucun, F. (2015). FT-IR and Raman vibrational analysis, B3LYP and M06-2X simulations of 4-bromomethyl-6-tert-butyl-2H-chromen-2-one. *Journal of Molecular Structure*, *1079*, 194–202.

Sert, Y., Singer, L. M., Findlater, M., Doğan, H., & Çırak, Ç. (2014). Vibrational frequency analysis, FT-IR, DFT and M06-2X studies on tert-Butyl N-(thiophen-2yl)carbamate. *Spectrochimica Acta Part A: Molecular and Biomolecular Spectroscopy*, *128*, 46–53.

Strathmann, T. J., & Myneni, S. C. B. (2004). Speciation of aqueous Ni(II)-carboxylate and Ni(II)-fulvic acid solutions: Combined ATR-FTIR and XAFS analysis. *Geochimica et Cosmochimica Acta*, *68*, 3441–3458.

Sutton, C. C. R., Franks, G. V., & da Silva, G. (2015). Modeling the antisymmetric and symmetric stretching vibrational modes of aqueous carboxylate anions. *Spectrochimica Acta Part A: Molecular and Biomolecular Spectroscopy*, *134*, 535–542.

Turner, J. V., & Agatonovic-Kustrin, S. (2007). 5.29—In silico prediction of oral bioavailability. In J. B. Taylor & D. J. Triggle (Eds.), *Comprehensive Medicinal Chemistry II* (pp. 699–724). Elsevier.

Ünal, Y., Nassif, W., Özaydin, B. C., & Sayin, K. (2021). Scale factor database for the vibration frequencies calculated in M06-2X, one of the DFT methods. *Vibrational Spectroscopy*, *112*, 103189.

Winiwarter, S., Ridderström, M., Ungell, A.-L., Andersson, T. B., & Zamora, I. (2007). Use of molecular descriptors for absorption, distribution, metabolism, and excretion predictions. In J. B. Taylor & D. J. Triggle (Eds.), *Comprehensive Medicinal Chemistry II* (pp. 531–554). Elsevier.

Yang, W., & Parr, R. G. (1985). Hardness, softness, and the fukui function in the electronic theory of metals and catalysis. *Proceedings of the National Academy of Sciences*, *82*(20), 6723–6726.

Zaater, S., Bouchoucha, A., Djebbar, S., & Brahimi, M. (2016). Structure, vibrational analysis, electronic properties and chemical reactivity of two benzoxazole derivatives: Functional density theory study. *Journal of Molecular Structure*, *1123*, 344–354.

Zhao, Y., & Truhlar, D. G. (2008). The M06 suite of density functionals for main group thermochemistry, thermochemical kinetics, noncovalent interactions, excited states, and transition elements: Two new functionals and systematic testing of four M06-class functionals and 12 other functionals. *Theoretical Chemistry Accounts*, *120*(1), 215–241.

Author Information

Manel Taferguennit	**Noura Kichou**
University of Sciences and Technology Houari Boumediene BP 32, 16111 Algiers, Algeria. Contact e-mail: *mtaferguennit@usthb.dz*	University of Mouloud Mammeri of Tizi-Ouzou, Tizi-Ouzou, Algeria.

Zakia Hank
University of Sciences and Technology Houari Boumediene
BP 32, 16111 Algiers, Algeria.

To cite this article:

Taferguennit, M., Kichou, N., & Hank, Z. (2023). Comparative experimental and theoretical study on the structure of potassium 2,4-hexadienoate:structure-activity relationship. *The Eurasia Proceedings of Science, Technology,Engineering & Mathematics (EPSTEM), 23,* 69-84.